

Magnetic Characterization of Powder Samples
from the Magnetocaloric compound
Series $\text{Mn}_{5-x}\text{Fe}_x\text{Si}_3$

Bachelorarbeit

von

Hang Zong

vorgelegt der

FACHHOCHSCHULE AACHEN

AACHEN UNIVERSITY OF APPLIED SCIENCES

Fachbereich Energietechnik

Studiengang Elektrotechnik

Im August 2016

angefertigt am

Jülich Centre for Neutron Science JCNS und Peter Grünberg Institut PGI
Forschungszentrum Jülich GmbH
Forschungszentrum Jülich

Prof. Dr. A. Förster
Dr. habil. K. Friese
P. Hering

Prüfer 1: Prof. Dr. Arnold Förster

Prüfer 2: Dr. Karen Friese

Betreuer: Paul Hering

Hiermit versichere ich, dass diese Arbeit ist von mir selbständig angefertigt und verfasst worden. Es sind keine anderen als die angegebenen Quellen und Hilfsmittel verwendet worden.

Ort, den Datum

Unterschrift: Hang Zong

Contents

Introduction	1
1. Theory	
1.1 The Magnetocaloric Effect	2
1.2 Magnetic phases	4
1.3 Requirements to a promising magnetocaloric material	8
1.4 State of the art research on the compound system $Mn_{5-x}Fe_xSi_3$	9
2. Instrumentation	
2.1 Physical Property Measurement System	11
2.2 Vibrating Sample Magnetometer	13
3. Experimental	
3.1 Synthesis of the polycrystalline sample	16
3.2 Preparation of the samples for the magnetic measurements	19
3.3 Experimental procedures for the magnetic measurements	21
3.4 Description of example sequence files	22
3.5 Summary of all measurements	26
4. Results and Analysis	
4.1 Data preparation	27
4.2 Discussion of magnetic properties of $Mn_{3.5}Fe_{1.5}Si_3$	30
4.3 Discussion of magnetic properties of $Mn_{2.5}Fe_{2.5}Si_3$	33
4.4 Discussion of magnetic properties of $Mn_{1.5}Fe_{3.5}Si_3$	37
5. Conclusions	41
Acknowledgements	44
Bibliography	46

Introduction

The magnetocaloric effect, i.e. the change of magnetic entropy and adiabatic temperature following a change in an applied magnetic field, forms the basis of magnetocaloric refrigeration technologies [1]. Magnetic refrigeration holds the potential to replace conventional vapor compression cooling [2]. It promises a lower energy consumption and it does not require the use of ozone depleting or other environmental hazardous gases. As requirements for magnetocaloric materials are demanding the search for suitable materials is ongoing.

The magnetocaloric compounds within the system $\text{Mn}_{5-x}\text{Fe}_x\text{Si}_3$ undergo a variety of magnetic phase transitions at different temperatures depending on their iron content [3]. Therefore, this system is a good candidate to develop a better understanding of the underlying mechanism of the MCE in multiple site driven magnetocaloric materials.

A published magnetic phase diagram describes the magnetic phases of the compounds $x=0, 1, 2, 3, 4$ and 5 [3]. The aim of this work is to characterize the intermediate compositions $x=1.5, 2.5$ and 3.5 with respect to their magnetism and compare the results with the existing phase diagram. This will help advancing the understanding the dependency of magnetic interactions and transition temperatures in relation to the iron content of the whole series even more.

1.Theory

1.1 The Magnetocaloric Effect

The Magnetocaloric Effect (MCE), is a physical phenomenon that allows certain kinds of material to absorb or release heat from its surrounding when a changing an magnetic field is applied i.e. the MCE is characterized by a change of magnetic entropy and temperature upon a change of the external field.

The explosion of global population and rapid environmental pollution lead to the Montreal Agreement (2000) where 194 countries declare to gradually forbid to massively produce or use Freon for refrigeration [4]. Magnetic cooling devices based on magnetocaloric materials hold the potential to replace conventional cooling technology by not only having the advantage of a gas free cycle, but also an increased efficiency by 20% ~ 30% compared to conventional gas compression cooling [5].

The general working theory of the MCE is the interplay between thermal motion, which happens inside the crystallographic structure (lattice entropy) and magnetic ordering (magnetic entropy). The following describes a magnetic cooling cycle step by step:

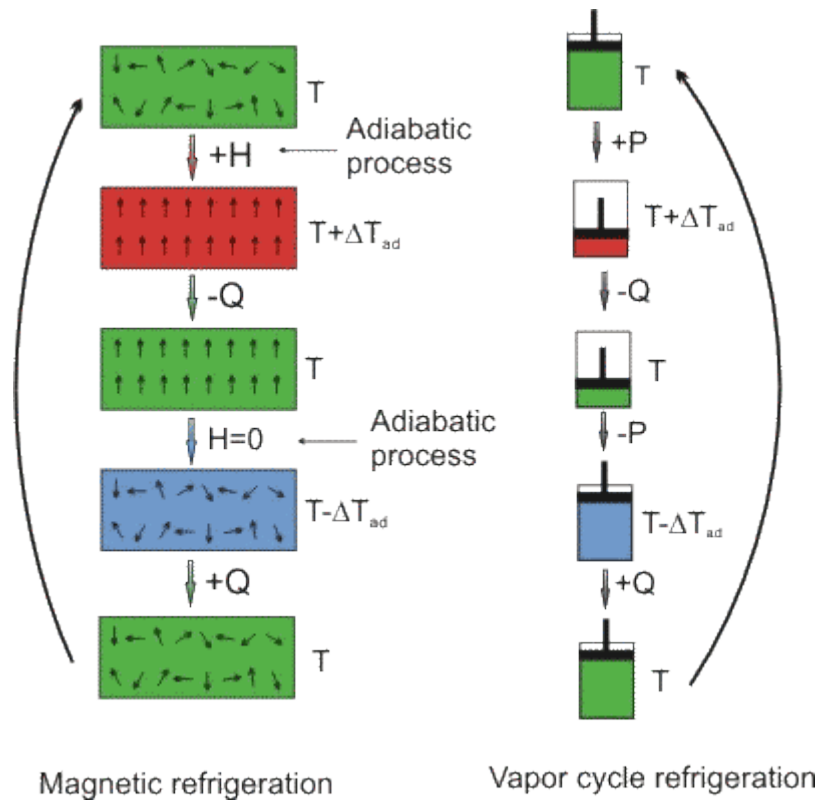


Figure 1. A comparison of the magnetic cooling cycle and traditional vapor compression cooling cycle [6].

A magnetic material is placed in an environment where it can be influenced by an external magnetic field in adiabatic conditions. With the appliance of the external field the magnetic entropy is decreased and as a result, following the law of thermodynamics, the lattice entropy is increased in the form of an increased temperature (Step 1). This heat is taken away by e.g. an exchange medium like water (Step 2). The external field is then removed adiabatically, causing magnetic disorder accompanied by an increased of magnetic entropy and a decrease in lattice entropy (Step 3). As a consequence the materials can now absorb heat from its surrounding, so the temperature of the environment drops down (Step 4). This magnetic refrigeration cycle is repeated several times per second to realize magnetic cooling in application (Step 5).

1.2 Magnetic phases

The MCE shows a maximum at magnetic phase transitions and is closely related to magnetic ordering. Therefore, in the following 4 basic magnetic states will be briefly explained: paramagnetism, diamagnetism, ferromagnetism and antiferromagnetism.

Paramagnetism

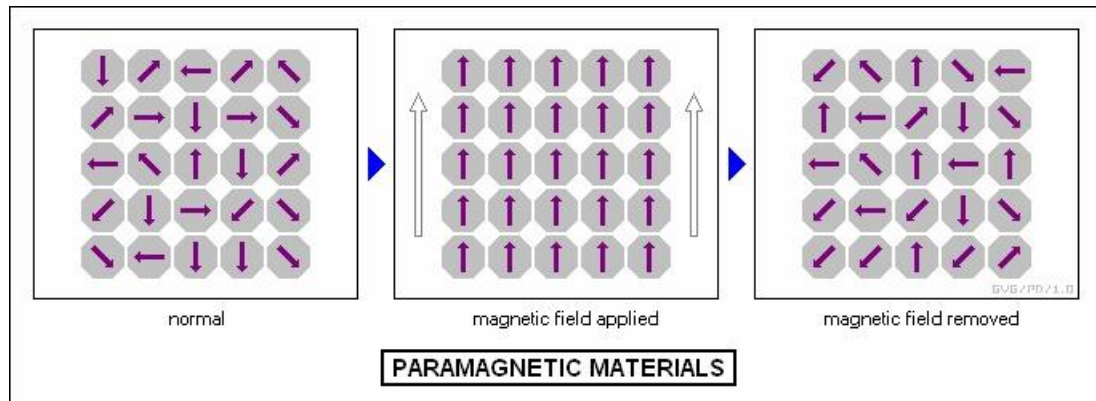


Figure 2. Schematic drawing of the response of the internal magnetic moments in a paramagnetic material to an applied/removed magnetic field. [7]

Paramagnetism describes the response of a class of materials to an externally applied magnetic field and represents one of the classes of magnetic phases. Each atom in a paramagnet carries a spin. In the absence of a magnetic field, they are randomly oriented. With the appliance of an external magnetic field the internal magnetic moments align in the direction of the field. As a result the total magnetic field inside the material is higher than outside. Paramagnetic materials generally have a magnetic permeability (μ_r) which is greater or at least equal to 1 and follow Curie's law:

$$M = \chi \cdot H$$

With: M = magnetization

χ = magnetic susceptibility

H = externally magnetic field

The explanation for the existence of microscopic moments in paramagnetic materials is the presence of unpaired electrons. This is dependent on the electron configuration of the chemical elements in it. For example, typical paramagnetic materials contain magnesium, molybdenum, lithium, or tantalum.

Diamagnetism

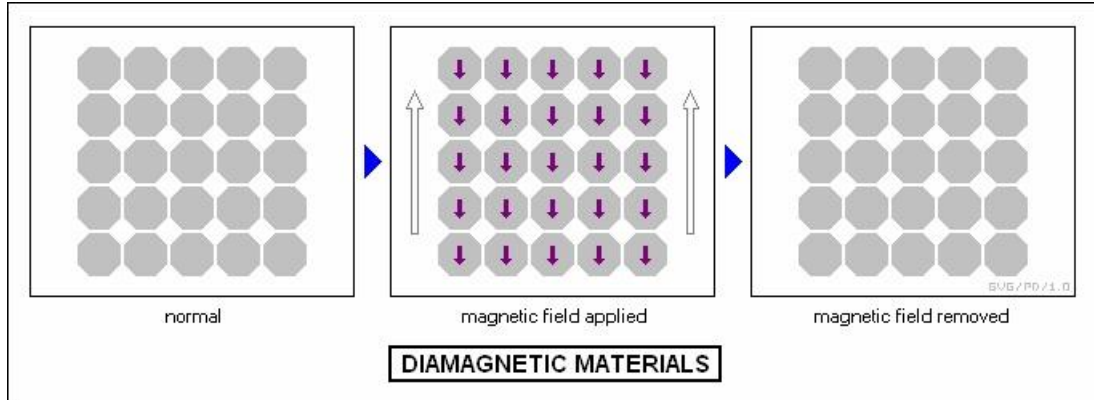


Figure 3. Schematic drawing of the response of internal magnetic moments in a diamagnetic material to an applied/removed magnetic field. [7]

Diamagnetism describes the response of another class of materials to an externally applied magnetic field and also represents one of the classes of magnetic phases. The atoms in diamagnetic materials do not carry a magnetic moments. In an external magnetic field microscopic moments are induced and order therefore antiparallel to the external field. This means the magnetic field inside the material is pointing in the opposite direction to the applied magnetic field (see fig. 3).

All materials show diamagnetism in an applied magnetic field. The effect of diamagnetism is very small compared to the ones of paramagnetism and ferromagnetism. Therefore, diamagnetism can be neglected in materials that also show paramagnetism or ferromagnetism. Only materials with completely paired up electrons are considered as diamagnetic materials and have magnetic susceptibility smaller 1:

$$\mu_r = \mu / \mu_0,$$

$$\chi_m = \mu_r - 1$$

with: μ_r = relative permeability

μ = permeability of a specific medium

μ_0 = permeability of free space

χ_m = magnetic susceptibility

Ferromagnetism

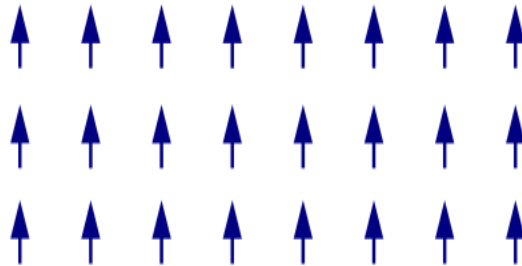


Figure 4. Schematic drawing illustrating the ordering of the microscopic magnetic moments in ferromagnetic materials.

In contrast to paramagnetic and diamagnetic materials, ferromagnetic materials show a stable parallel ordering of the internal microscopic moments without an applied external field. This means they passively have an intrinsic magnetic field called coercive field. Ferromagnetic materials have a magnetic permeability (μ_r) which is much bigger than one.

The ordering is caused by exchange interactions between the electrons in a material that are sufficiently large to overcome the thermal disorder in the system. The exchange interaction between the electrons is dependent on the electron configuration. At room temperature only iron, nickel and cobalt show ferromagnetism.

Every ferromagnetic material has a specific temperature at which the ordering collapses due to the increase of thermal disorder. This critical temperature is called Curie-Temperature.

Antiferromagnetism

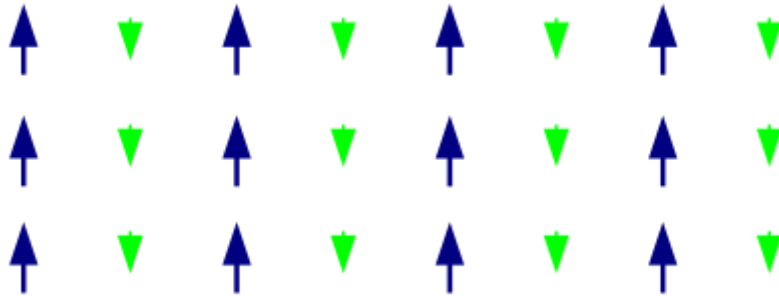


Figure 5. Schematic drawing of the ordering of the microscopic magnetic moments in antiferromagnetic materials.

Antiferromagnetic materials show a stable ordering of the internal microscopic moments, which is not parallel and exists without an applied external field. The individual internal moments are aligned at an angle different to 0° in a way that they partly or completely compensate each other over the whole crystal. An example of an antiferromagnet is a material where the spins on two different sublattices exhibit antiparallel ordering to each other. The magnetic susceptibility of an antiferromagnetic material is very close to 0.

Similar to ferromagnetic materials the ordering originates from a correlated electron system. The critical temperature in antiferromagnetic materials, where the magnetic order breaks down, is called Néel-temperature.

1.3 Requirements for a promising magnetocaloric material

Since the focus on magnetic refrigeration has emerged with the discovery of the giant MCE in $\text{Gd}_5\text{Si}_2\text{Ge}_2$ in 2001 [8], scientists made big efforts in the search for the best material for application. The demands on a suitable material are diverse [5]:

- 1) The changes in magnetic entropy ΔS_M and adiabatic temperature ΔT_{ad} should be as large as possible around the transition temperature,
- 2) As a consequence, a large density of magnetic moments in the material is necessary.
- 3) The lattice entropy should be small,
- 4) The transition temperature should be at working temperatures of domestic cooling devices i.e. close to room temperature
- 5) A small thermal hysteresis is necessary to minimize losses due to latent heat.
- 6) A low specific heat capacity and high thermal conductivity is necessary to realize a good heat exchange with the transport medium.
- 7) Reliable chemical stability and ease of synthesis are key for an application of the material.
- 8) The used elements should be cheap, abundant, and non-toxic.

1.4 State of the art of research on the compound system

$\text{Mn}_{5-x}\text{Fe}_x\text{Si}_3$

The compounds within the system $\text{Mn}_{5-x}\text{Fe}_x\text{Si}_3$ have the advantage that they do not contain expensive rare earth elements like Gd, nor toxic elements like As. Hexagonal structural models were published for the compounds $x=0, 1, 2, 3$ and 4 refined in space group $P6_3/mcm$ [9]. The structure of the compound MnFe_4Si_3 was later redetermined in space group $P-6$ [10].

Within the structure two symmetrically independent sites exist for Mn and Fe. Depending on the composition, the sites are either purely occupied by Mn or Fe, or they show mixed occupancy by Mn and Fe. Magnetic data are published for all compounds with $x=0, 1, 2, 3, 4$ and 5 [3]. The compounds undergo a variety of magnetic phase transitions at different temperatures depending on their iron content (Figure 6). The corresponding magnetic entropy changes show different shapes and magnitudes ranging from a negative MCE ($x=0$) to the modestly high positive magnetocaloric effect (MCE) of 2.9 J/kg K at a magnetic field change from 0 T to 2 T for $x=4$. Therefore, this system is an ideal choice to gain a better understanding of the underlying mechanism of the MCE in multiple site driven magnetocaloric materials.

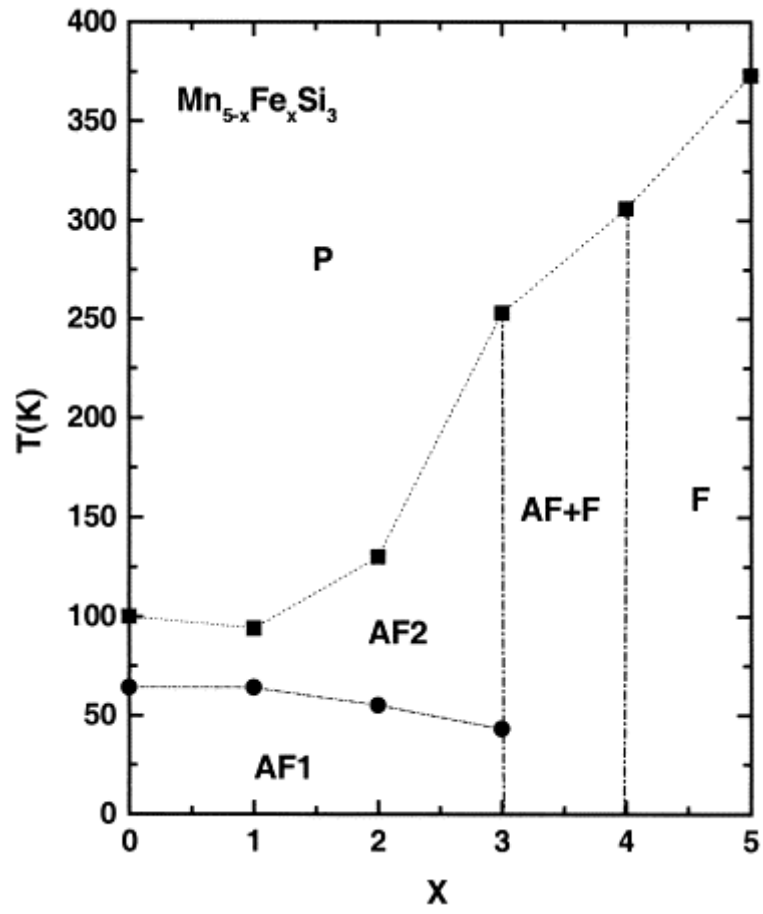


Figure 6. Sketch of the magnetic phase diagram of the $\text{Mn}_{5-x}\text{Fe}_x\text{Si}_3$ series for compounds $x=0, 1, 2, 3, 4$ and 5 according to [3]

2. Instrumentation

2.1 Physical Property Measurement System

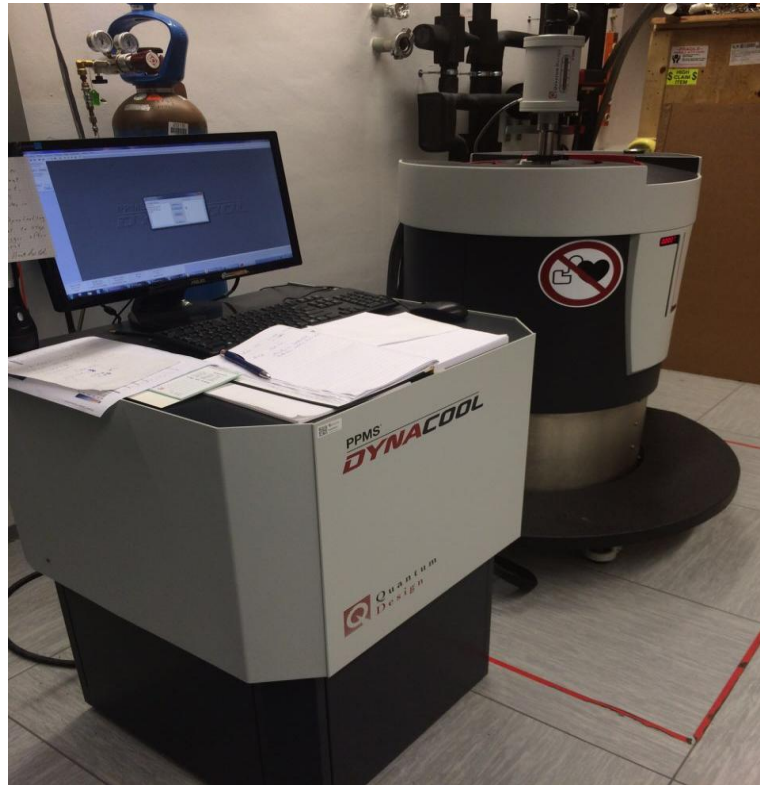


Figure 7. Used Physical Property Measurement Systems, Dynacool.

All measurements of the macroscopic magnetic properties were performed on a Physical Property Measurement System Dynacool by Quantum design (Figure 7).

The general system includes the following features:

- Temperature Control System
- Superconducting Magnet System
- Research Dewar
- Model 6000 Control Center
- MultiVu Software Interface

A list of available measurement options is given below:

- Low temperature stages
- Thermal measurements
- Magnetometry (Torque Magnetometry, AC Susceptibility, Magneto-Optic and Vibrating Sample Magnetometer (VSM))
- Electro-Transport
- Microscopy
- High Pressure
- Spectroscopy

The used systems allow for a well-controlled sample environment in the temperature range from 1.9K to 400K and external magnetic field strengths in the range from -9T to 9T.

2.2 Vibrating Sample Magnetometer



Figure 8.
Simon Foner[11]

A Vibrating Sample Magnetometer (VSM) comes as one of the measurement options of the PPMS to measure magnetic properties such as hysteresis loop, initial magnetization curve, demagnetization curve, IRM (Isothermal Remanent Magnetization) and DCD (DC demagnetization) curves. Modern vibrating sample magnetometer is considered to be invented in the year of 1955 by Simon Foner at Lincoln Laboratory, MIT, USA.

The sample is placed in a magnetically homogeneous sample holder to minimize magnetization from the holder. The holder is mounted to a sample rod which then is driven by VSM linear motor, which is responsible for the vibrating movement. A superconducting magnet is used to surround the sample in homogeneous magnetic fields during the measurement. Measurements are conducted by performing a sinusoidal movement in the surrounding of a pickup coil. According to the Faraday Law of electromagnetic induction, a induced voltage is generated and detected. Magnetic properties like magnetization and hysteresis curve of the sample thus are measured by converting the sample dipole field into an AC-electrical signal. In order to get an accurate signal an oscillation amplitude with a peak of 1-3 mm and a frequency of 40 Hz is usually applied. A sensitivity to magnetization changes in the range of $<10^{-6}$ emu at a data rate of 1 Hz could be reached [12]. Fig. 9 shows a schematic structure of the used VSM magnetometer. It consists of the following parts:

- A. VSM linear motor to vibrate the sample,
- B. Pick-up Coils for detection,
- C. Electronics for driving the linear motor and detect the magnetic response through the pick-up coils.

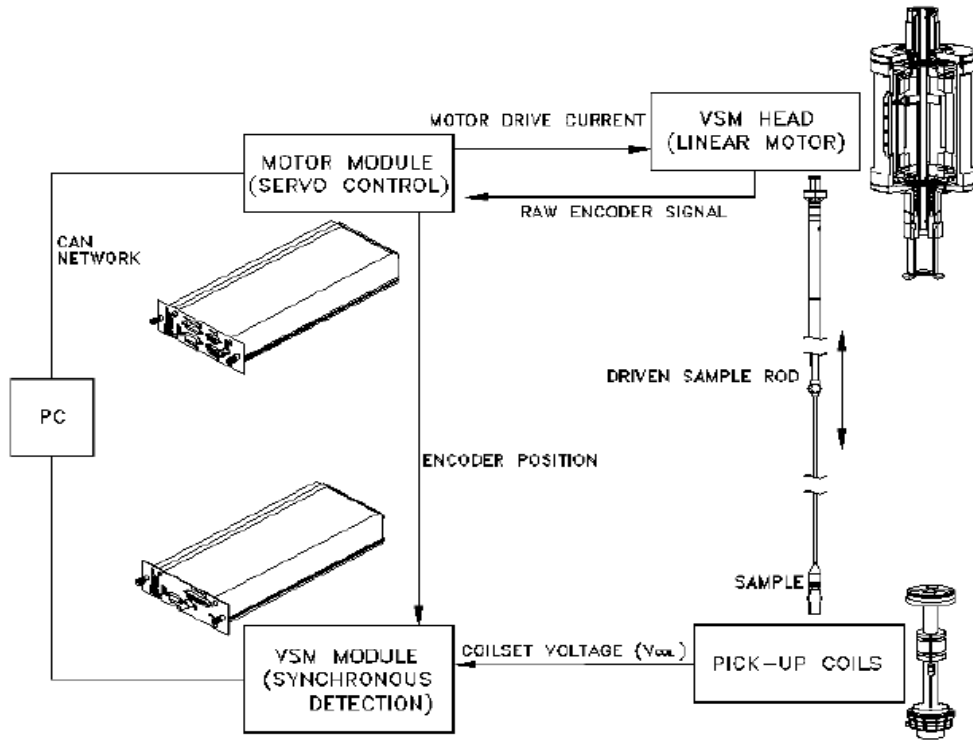


Figure 9. Schematic drawing of the used VSM magnetometer [13]

As mentioned before, the fundamental theory of the VSM magnetometer is based on Faraday's laws: a voltage is induced in the pick-up coils by the change of magnetic flux through movement of sample in the applied magnetic field. The following equation shows the mathematical relationship between magnetic flux, time and voltage induced:

$$V_{\text{coil}} = \frac{d\Phi}{dt} = \left(\frac{d\Phi}{dz} \right) \left(\frac{dz}{dt} \right)$$

with:

Φ : magnetic flux enclosed by the pickup coil

z : vertical position of the sample

In the case of a vibrational movement a better description of their relationship can be derived as:

$$V_{\text{coil}} = 2\pi f \cdot C \cdot m \cdot A \cdot \sin(2\pi ft)$$

with:

C : coupling constant

m: magnetic moment of the sample

A: amplitude of sinusoidal oscillation

f: frequency of oscillation, reciprocal of period.

Since all parameters except the magnetic moment are recorded during a measurement m can be derived.

3 . Experimental

3.1 Synthesis of the polycrystalline samples

All polycrystalline samples of the series $Mn_{5-x}Fe_xSi_3$ were synthesized by the cold crucible induction melting process (Figure 11). The prepared stoichiometries are $Mn_{3.5}Fe_{1.5}Si_3$, $Mn_{2.5}Fe_{2.5}Si_3$ and $Mn_{1.5}Fe_{3.5}Si_3$.

First we weighed the three pure elements Fe, Mn and Si according to the respective mass ratio in the compounds. They were placed in a copper crucible using tweezers in order to prevent any possible contamination. Special attention needed to be paid to the slits in the base of the copper crucible to avoid small pieces of raw materials to fall down. Big pieces were placed at the bottom allowing the smaller pieces to be placed safely on the top. To prevent oxidation the ingots were first sealed in the sample chamber then evacuated to 10^{-6} mbar and finally the sample chamber was filled with argon till ambient pressure was reached. In the next step, the samples were melted in the water cooled crucible followed by inducing currents in the samples (Figure 12). The induced currents heated the elements over their melting temperature as well as levitating and blending the melt. To further improve the homogeneity of the samples the cooled melts were turned around and melted again for three times. All three samples, have the same preparation process. They only difference being the amount of each element before the melting according to the required stoichiometry.

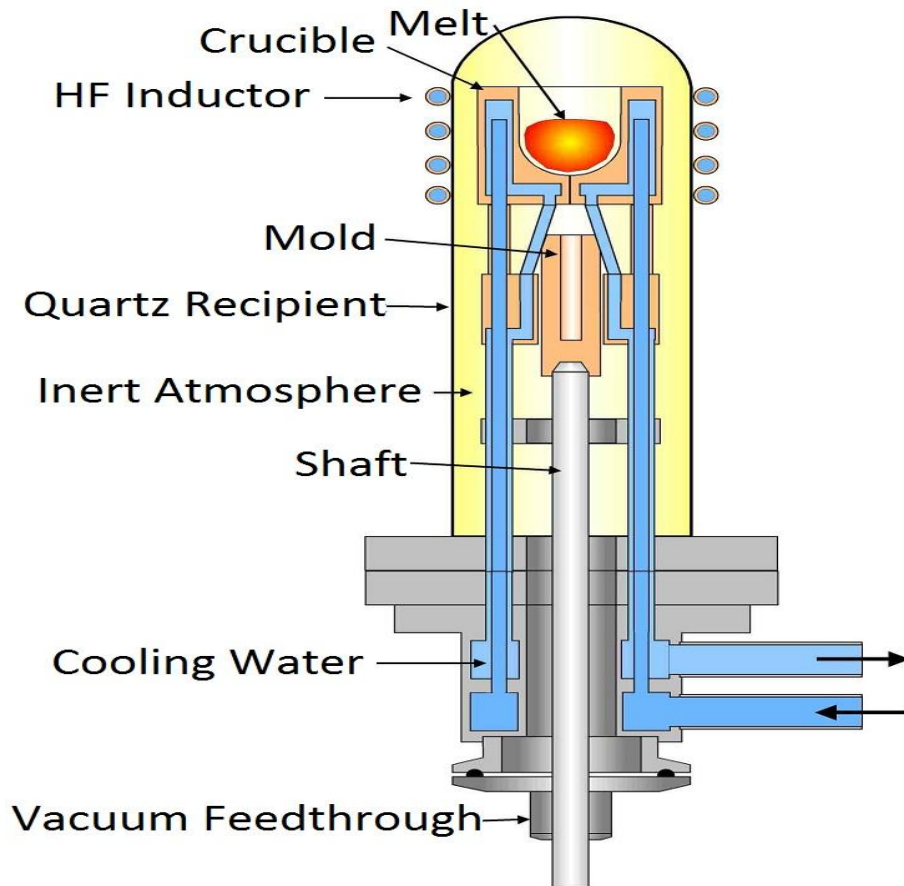


Figure 10. Schematic structure of the cold crucible induction melting instrument [14]

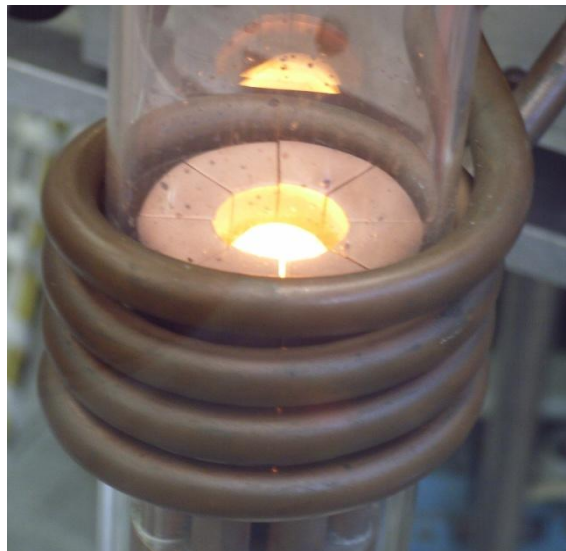


Figure 11. Melting process of the material in the cold crucible during induction melting.

After the cold crucible induction melting process all samples were grinded by hand in a mortar until they did not show metallic glimmering anymore. A picture of the powder sample is shown in Figure 11.



Figure 12. Polycrystalline Sample of the $\text{Mn}_{5-x}\text{Fe}_x\text{Si}_3$ Series produced by cold crucible melting after the grinding process.

3.2 Preparation of the samples for the magnetic

measurements

Before filling in the sample we carefully cleaned the polypropylene sample holder meant for macroscopic magnetization measurements in the VSM option of the PPMS. In order to avoid any possible contamination from the experimenter, we conducted all steps wearing rubber disposable glove. The two part sample holder was cleaned inside and outside using isopropyl, paper towels and toothpicks. After the process it was dried in the air. In the next step, the net weight of the empty polypropylene powder holder without any sample was determined with the help of an electronic balance. In order to transfer the powder sample into the powder holder, we used two different ways. The first method consisted in using a small spoon to transfer small amounts of powder into the holder, followed by cleaning the powder off, which fell out of the powder holder during the filling. Then we closed the sample holder and compressed the powder. The second method consisted in making a little funnel with paper and filling the powder through it into the sample holder.

After filling the powders to the sample holders they were weighted again to determine the sample mass by subtracting the mass of the empty sample holder from the mass of the filled one. The sample masses are shown in tab. 1. A precise determination of the mass of the sample is necessary, as the mass of the samples is used for the normalization of the magnetic moment (emu) to the mass magnetization (Am^2/kg).

Variable x	Sample	Mass(mg)
X=1.5	$\text{Mn}_{3.5}\text{Fe}_{1.5}\text{Si}_3$	26.3
X=2.5	$\text{Mn}_{2.5}\text{Fe}_{2.5}\text{Si}_3$	12.1
X=3.5	$\text{Mn}_{1.5}\text{Fe}_{3.5}\text{Si}_3$	14.1

Table 1. Masses of the $\text{Mn}_{5-x}\text{Fe}_x\text{Si}_3$ samples for the magnetic measurements

In order to mount the polypropylene sample holder to the sample rod of the PPMS,

Quantum Design provides a brass cartridge that can be screwed to the rod. It is pated with cobalt hardened gold and has a small magnetic background signal. The polypropylene sample holder slides into the brass cartridge. By using the mounting station it can be moved to the correct position inside the pickup coil range when inserted to the PPMS (see fig. 13).

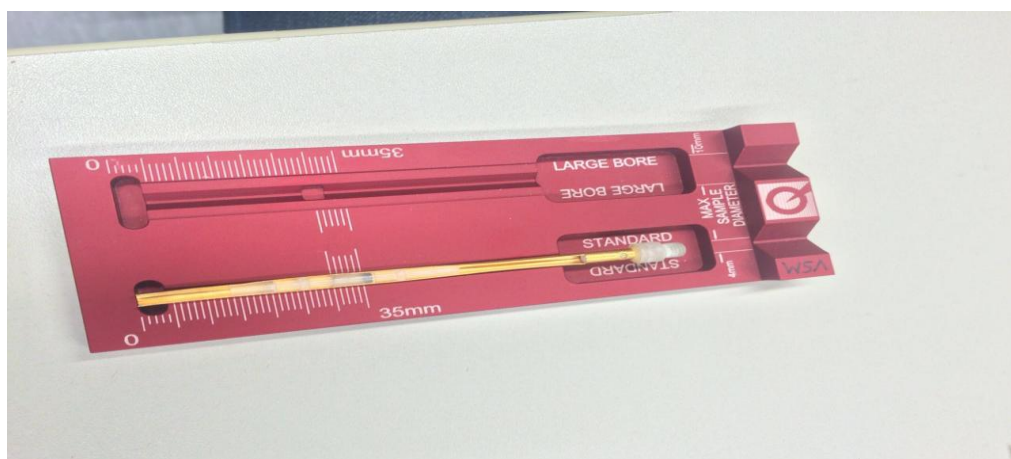


Figure 13. Mounting station to center the polypropylene sample holder with the sample at the correct position.

After screwing the brass cartridge to the sample rod it is inserted into the PPMS sample chamber which is then covered. The exact sample position was determined by the internal centering procedure of the PPMS using a small field of 50 Oe to enhance the signal of the sample. With this done the sample chamber was sealed and purged with helium. Files containing the sequences of the measurements were created to define the experimental procedure.

3.3 Experimental procedures for the magnetic measurements.

Two types of magnetic moments measurements were conducted:

Isothermal:

During the whole process of this measurement mode, the temperature is kept constant while the magnetic field is changed. For the first part, the so- called virgin curve, the field is increased from 0 T to 0.5 T. From there it is cycled to -0.5 T and back to 0.5 T. This measurement type is able to discover field driven magnetic transitions, saturation magnetization and remanence. A plot of the magnetic field versus the measurement time is shown in Fig. 14.

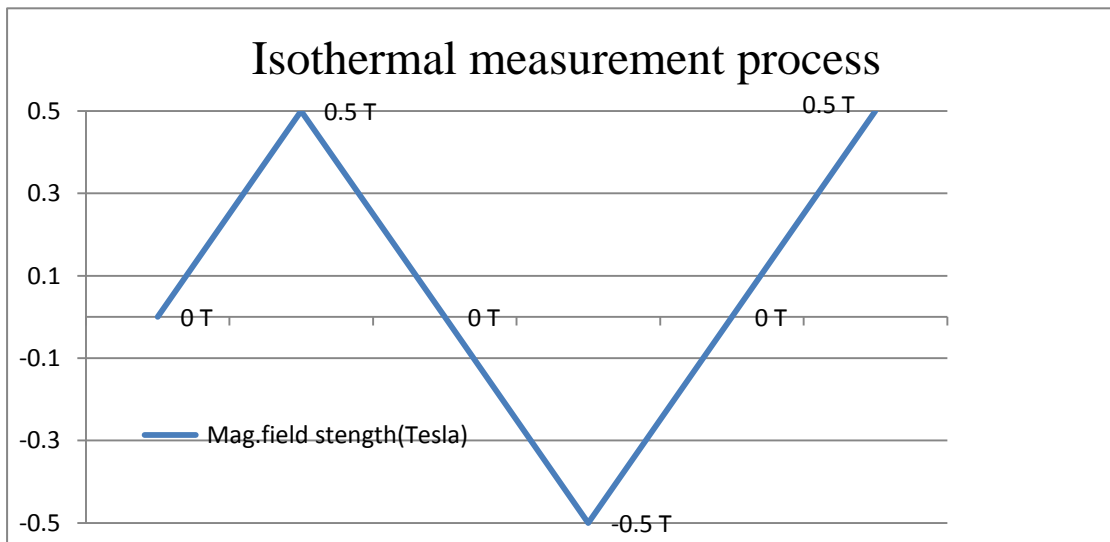


Figure 14. Typical variation of the magnetic field versus the measurement time in an isothermal measurement of the magnetic moment.

Isofield:

Isofield means the sample is kept in an environment of constant magnetic field. For our measurements we used the following fields: 0.3 T, 0.6 T, 0.9 T, 1.2 T, 1.5 T and 1.8 T. The magnetic moment is recorded during a temperature sweep from 10 K to 390 K and back to 10 K. This type of measurement is able to discover magnetic transition temperatures and types as well as thermal hysteretic behavior.

3.4. Description of example sequence files

Two representative measurement sequences for isothermal and isofield measurements are shown in the following:

Sequence of a complete isothermal measurement cycle and its steps:

“New Datafile “C:\QdDynacool\Data\Zong\MN25FE25SI3_390K.DAT”;

Assignment of path and filename.

“Set Magnetic Field 0.00 Oe at 100.0 Oe/sec, Linear”

Set the magnetic field to 0.00 Oe with a rate of 100.0 Oe/sec.

“Wait For Field, Delay 1 sec , No action”;

Wait for the field to reach 0 Oe, then wait 1 s.

“Set Temperature 390K at 12K/min. Fast settle”;

Set the temperature of 390K in a warm up speed of 12 K per minute to guarantee a known state in the paramagnetic regime at the beginning of the measurements.

“Wait For Temperature, Delay 60 seconds (1.0 mins), No actions”;

Wait for the chamber temperature to reach 390K, then wait 60 s to allow for a temperature equilibrium within the chamber and the sample.

“VSM Moment vs Field 5 Quadrants -5000 Oe to 5000 Oe Sweep Continuous AutoCenter ON”;

Start of the measurement process of the magnetic moment in a isothermal measurement with virgin curve part in the field range from -0.5 T to 0.5 T. The field is changed in a continuous sweeping motion during the measurement.

“Set Magnetic Field 0.00 Oe at 100.0 Oe/sec, Linear”

Set the magnetic field to 0.00 Oe with a rate of 100.0 Oe/sec to have a well-defined state after changing the temperature for the next measurement.

“Wait For Field, Delay 1 sec , No action”;

Wait for the field to reach 0 Oe, then wait 1 s.

“New Datafile “C:\QdDynacool\Data\Zong\MN25FE25SI3_300K.DAT”;

Start of the next measurement routine (at 300 K).

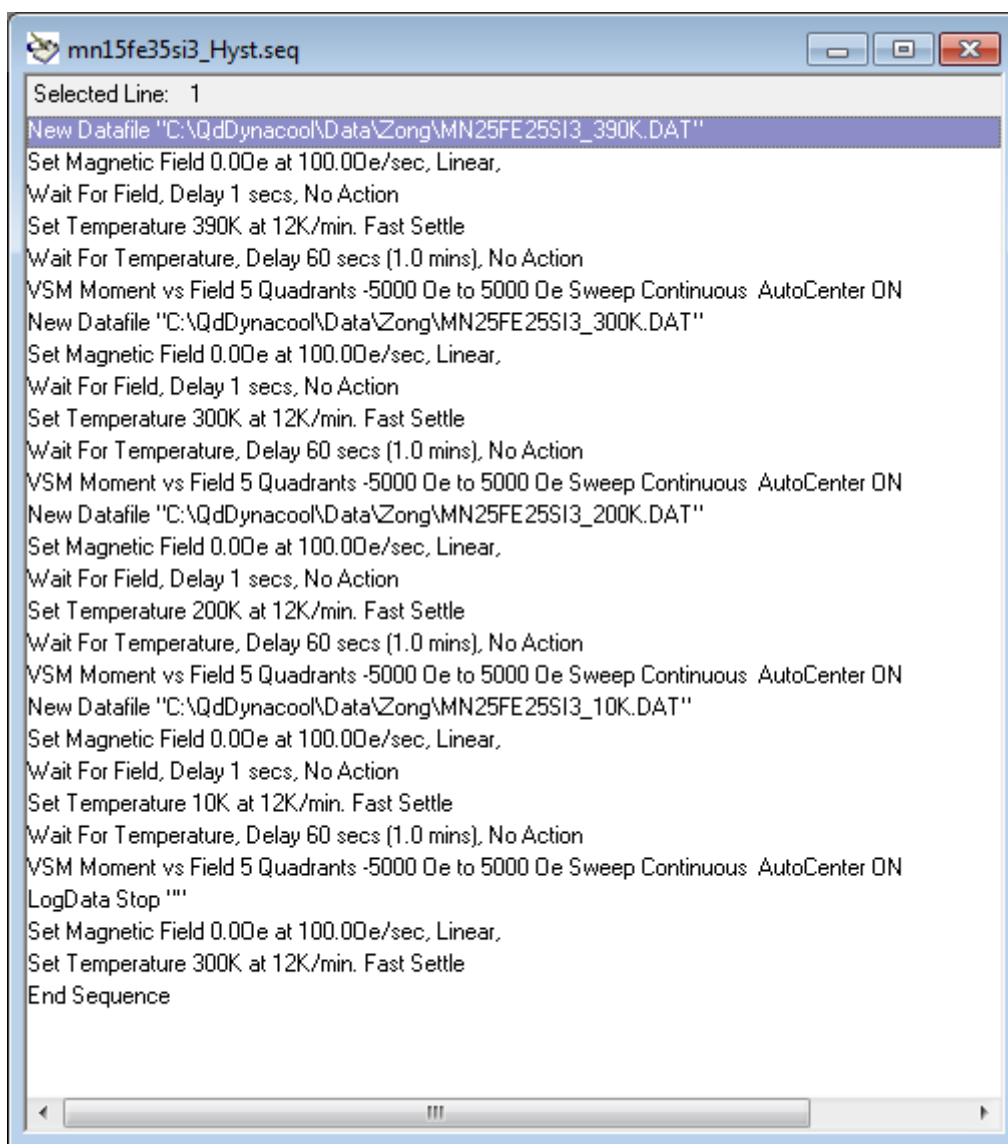


Figure 15. Screenshot of the measurement sequence of field dependent magnetic moments at different temperatures in $Mn_{2.5}Fe_{2.5}Si_3$.

Sequence of a complete isothermal measurement cycle and its steps:

“New Datafile “C:\QdDynacool\Data\Zong\MN25FE25SI3_100OE.DAT”;

Assignment of path and filename.

“Set Temperature 390K at 12K/min. Fast settle”;

Set the temperature of 390K in a warm up speed of 12 K per minute to guarantee a known state in the paramagnetic regime at the beginning of the measurements.

“Wait For Temperature, Delay 60 seconds (1.0 mins), No actions”;

Wait for the chamber temperature to reach 390K, then wait 60 s to allow for a temperature equilibrium within the chamber and the sample.

“Set Magnetic Field 100.0 Oe at 100.0 Oe/sec, Linear”

Set the magnetic field to 100.0 Oe with a rate of 100.0 Oe/sec.

“Set Temperature 10K at 10K/min. Fast settle”

Set the temperature to 10K. The instrument will cool down from 390K to 10K in a rate of 10K/min with an applied magnetic field (field cooled measurement).

“Wait for temperature, Field, Delay 60 secs (1.0 mins), No Action”.

Wait for a temperature equilibrium again.

“VSM Moment vs Temperature 10K to 390K Sweep Continuous AutoCenter ON”;

Start of the measurement process of the magnetic moment from 10K to 390K at a magnetic field strength of 100.0 Oe.

“Set temperature 390K at 12K/min. Fast settle”;

Stabilize the temperature at 390K.

“Wait for Temperature. Delay 60 secs (1.0 mins), No Actions”;

Wait for a temperature equilibrium.

“VSM Moment vs Temperature 390K to 10K sweep Continuous AutoCenterON”;

Measurement process of the magnetic moment from 390 K to 10 K at a magnetic field strength of 100.0 Oe.

“New Datafile “C:\QdDynacool\Data\Zong\MN25FE25SI3_3000OE.DAT”;

Start of the next measurement routine (at a magnetic field strength of 3000.0 Oe).

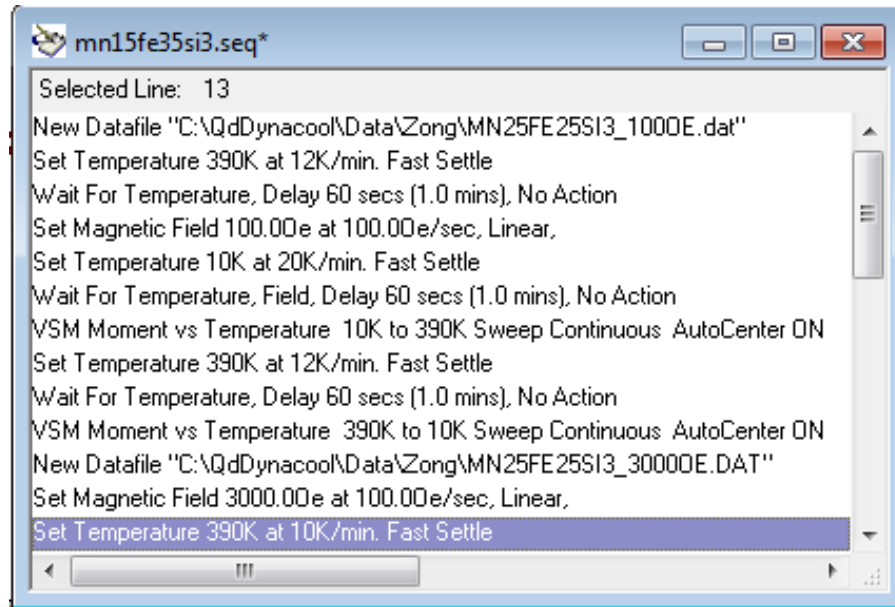


Figure 16. Screenshot of the measurement sequence of temperature dependent magnetic moments at different fields in $Mn_{2.5}Fe_{2.5}Si_3$.

3.5 Summary of all measurements

A list of all conducted measurements is given in the following table:

Sample	$\text{Mn}_{3.5}\text{Fe}_{1.5}\text{Si}_3$	$\text{Mn}_{2.5}\text{Fe}_{2.5}\text{Si}_3$	$\text{Mn}_{1.5}\text{Fe}_{3.5}\text{Si}_3$
Isofield:			
	10K \rightleftharpoons 390K	10K \rightleftharpoons 390K	10K \rightleftharpoons 390K
0.3T	✓	✓	✓
0.6T	✓	✓	✓
0.9T	✓	✓	✓
1.2T	✓	✓	✓
1.5T	✓	✓	✓
1.8T	✗	✓	✓
Isothermal:			
	-0.5T \rightleftharpoons 0.5T	-0.5T \rightleftharpoons 0.5T	-0.5T \rightleftharpoons 0.5T
200K	✗	✓	✓
300K	✗	✓	✓
390K	✗	✓	✓

Table 2. Table of all conducted measurements.

4. Results and Analysis

4.1 Data preparation

In order to prepare the measured data for further analysis they were first plotted with PPMS MultiVu Software [15] distributed with the PPMS.

All measured datasets consist of a column for temperature, one for magnetic field, one for total magnetic moment and one for the measurement error on the magnetic moment.

In the plots of these data we observed a series of erroneous data points resulting from a malfunction of the PPMS Dynacool. At low temperatures, below about 150 K, the pickup coil lost contact to the connection pins in the sample chamber. This bad electrical contact then lead to reduction of the measured magnetic moments. To identify all these bad data points we had a closer look into the measurements errors of all data points and found a strong correlation between large errors on the data points and the deviating data points with decreased magnetic moments. With this correlation in mind, we scanned all data for data points with strongly increased measurement errors and dismissed them. The threshold was set individually for each data set. An example of the measured data and the cleaned data is shown in Fig17 and Fig18.

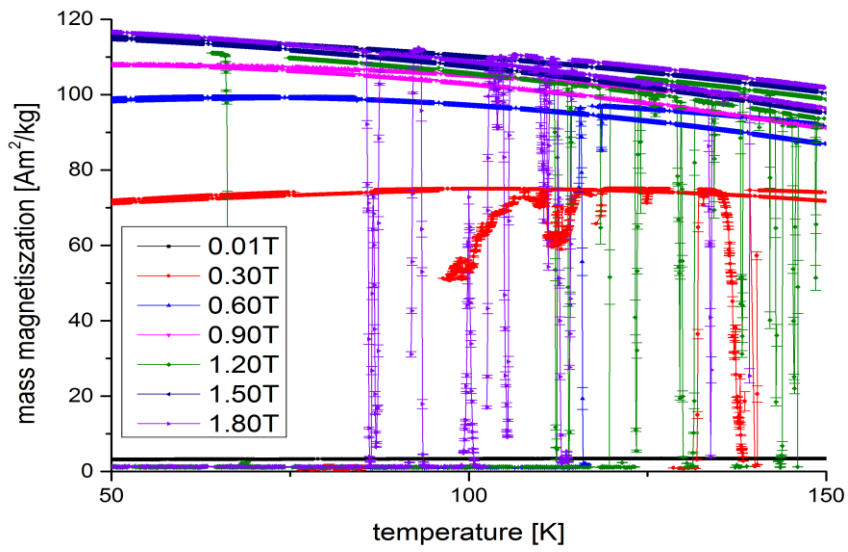


Figure 17. Original measurement result .

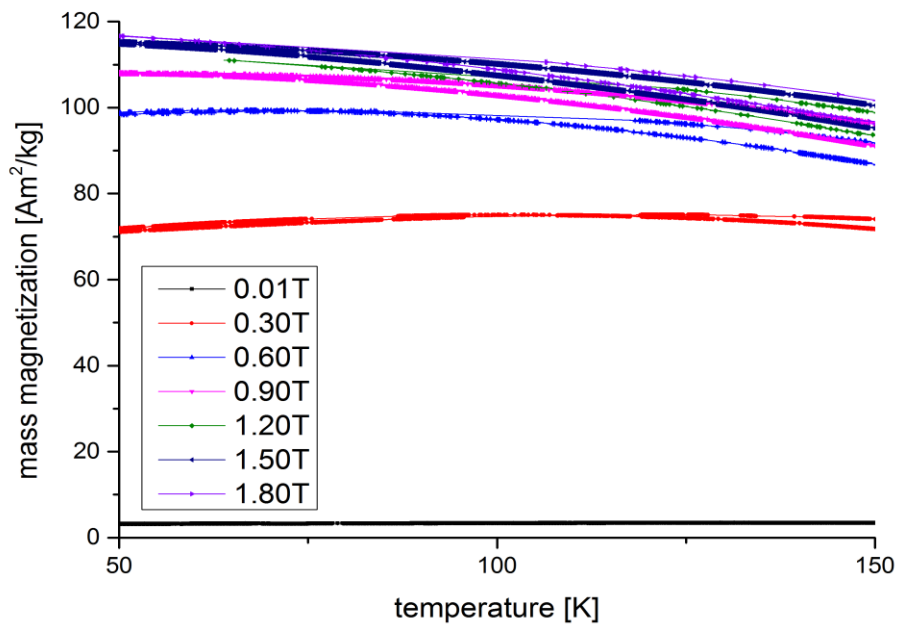


Figure 18. Improved measurement result after the error correlation.

In order to make the measurements comparable to previously published results as well as to each other we normalized the total magnetic moment and its error with the

sample mass. The following equation shows this conversion from total magnetic moment in emu to mass magnetization in Am²/kg:

$$\text{mass magnetization} = \frac{\text{magnetic moment}}{\text{mass}} = \frac{\text{A.m}^2}{\text{kg}} = \text{A}^* \text{m}^2 / \text{kg} = \frac{\text{emu}}{\text{g}}$$

with 1 A*m² = 10³ emu.

We also converted the unit for the external magnetic field from Oersted to Tesla with the following relation:

$$10000 \text{ Oe} = 1 \text{ T.}$$

After this preparation, all data were plotted with the program OriginPro 9 [16].

4.2 Discussion of magnetic properties of $\text{Mn}_{3.5}\text{Fe}_{1.5}\text{Si}_3$

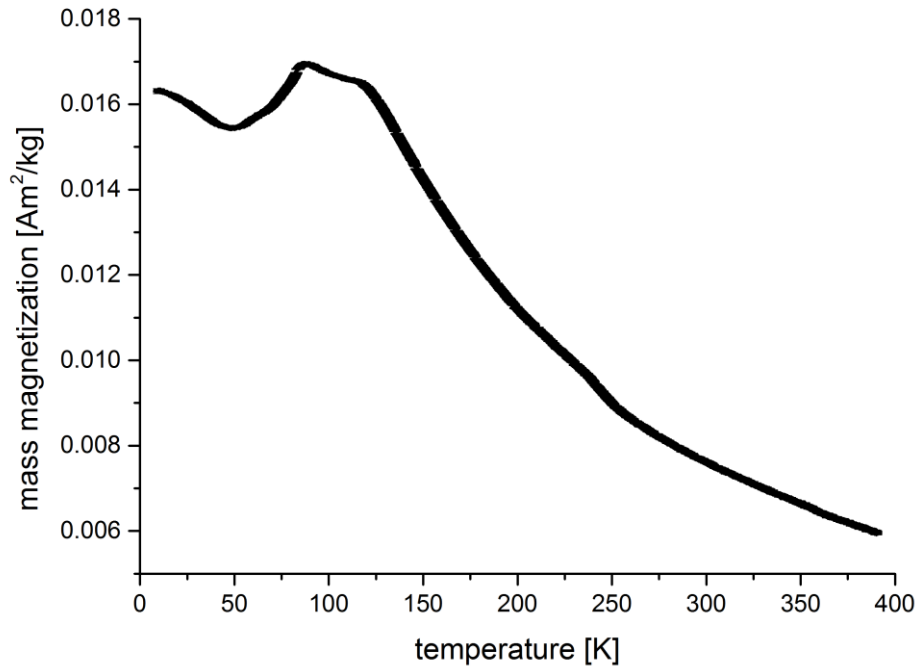


Figure 19. Isofield curve of $\text{Mn}_{3.5}\text{Fe}_{1.5}\text{Si}_3$ at 0.01 T.

Beginning with the isofield curve at the lowest measured external field where phase transitions are less smeared out the curve shows complex features. At low temperatures, the curve has a negative slope followed by a local minimum at $49 \text{ K} \pm 3 \text{ K}$. At higher temperatures there are two local maxima at $85 \text{ K} \pm 3 \text{ K}$ and $119 \text{ K} \pm 3 \text{ K}$ and then the curve continuously decays towards higher temperatures. The two local maxima at 85 and 115 K can be interpreted as two different antiferromagnetic phase transitions. The transition temperature fit well with the observed ones in the two compounds with adjacent compositions $x=1$ and $x=2$ [3]. The local minimum at low temperature (49 K) also hints towards a phase transition, yet here further investigations are necessary to allow for an unambiguous interpretation of its nature. .

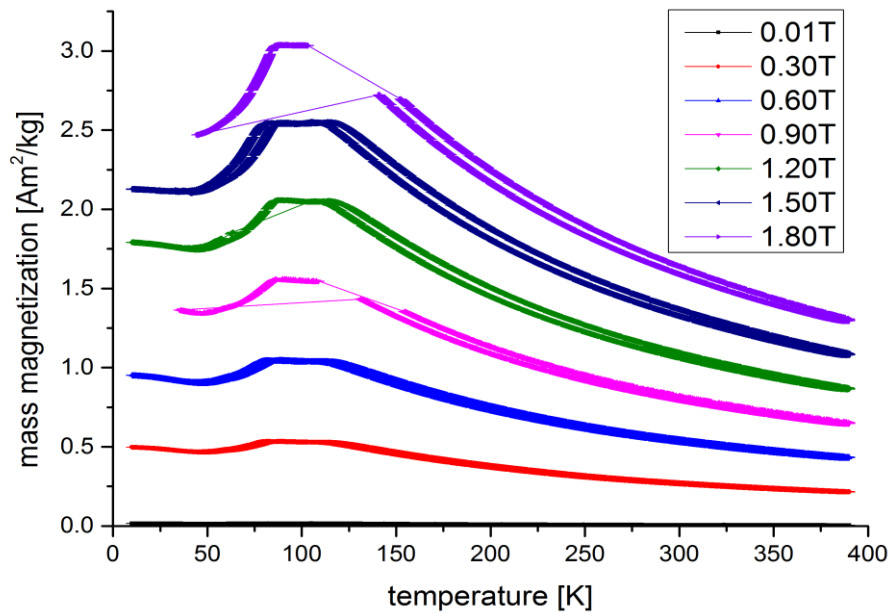


Figure 20. Isofield curves of $\text{Mn}_{3.5}\text{Fe}_{1.5}\text{Si}_3$ in different external magnetic fields.

At higher fields this local minimum vanishes completely. The two antiferromagnetic phase transitions, on the other hand, are still prominent and do hardly shift with fields towards higher or lower temperatures within the accuracy of the measurement. This can be seen in Fig. 21.

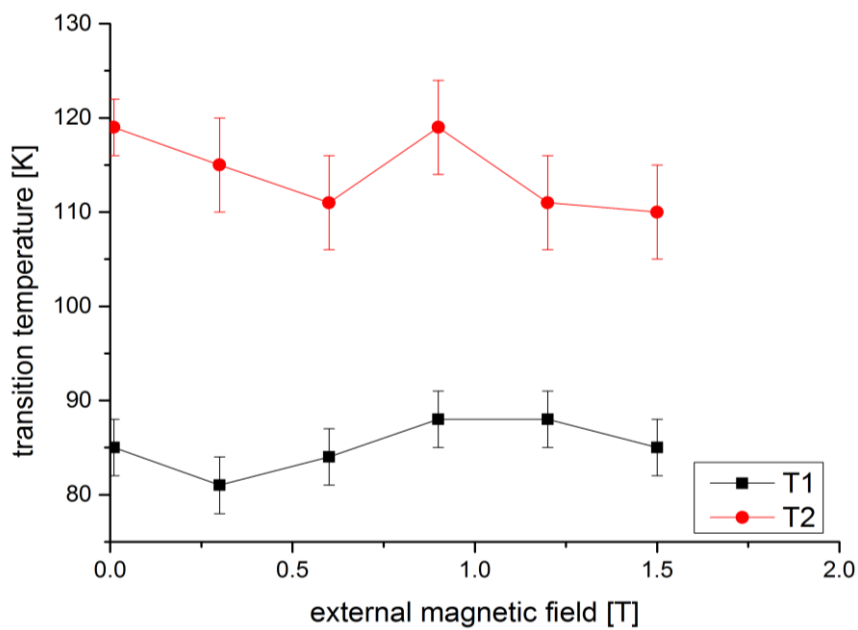


Figure 21. Transition temperatures of the two antiferromagnetic transitions in $\text{Mn}_{3.5}\text{Fe}_{1.5}\text{Si}_3$ and their dependency on the external magnetic field.

All curves at higher fields than 0.01 T show a splitting between the branch that was measured upon cooling when compared to the one measured upon heating. This thermal hysteresis starts to occur around 35 K and reaches a maximum of approximately $11 \text{ K} \pm 2 \text{ K}$ around 175 K. This maximum value stays constant throughout the field span from 0.3 T to 1.8 T. The maximum hysteresis splitting is shown in comparison with the other measured compounds in fig. 30. Towards higher temperatures the hysteresis splitting narrows down again. This variable size of the splitting as well as its absence in the 0.01 T curve show that it is a feature which can be attributed to the sample and does not originate from a non-equilibrated temperature in the sample chamber and sample trough due to a too fast temperature sweep rate.

Applying higher external fields also linearly increases the total value of the mass magnetization which for example has a maximum of $0.02 \text{ Am}^2/\text{kg} \pm 0.005 \text{ Am}^2/\text{kg}$ for an external field of 0.01 T and of $3.04 \text{ Am}^2/\text{kg} \pm 0.05 \text{ Am}^2/\text{kg}$ for an external field of 1.8 T.

4.3 Discussion of magnetic properties of $\text{Mn}_{2.5}\text{Fe}_{2.5}\text{Si}_3$

The curve for the isofield measurement of $\text{Mn}_{2.5}\text{Fe}_{2.5}\text{Si}_3$ at 0.01 T is missing all data points below about 125 K due to problems with instrument. A plot of this curve can be seen in Fig. 23. Due to time constraints and delays related to the repair of the instrument, the curve could not be remeasured.

Therefore we start describing the magnetic properties of $\text{Mn}_{2.5}\text{Fe}_{2.5}\text{Si}_3$ with the second lowest field measured. Here we performed a whole measurement cycle in the temperature range from 10 K to 390 K (Figure 23). The curve shows a slight increase of the mass magnetization from 10 K to a local maximum at $86 \text{ K} \pm 5 \text{ K}$ and a continuous decrease from there towards a flattening around 390 K. This decrease and flattening could also be observed in the only partly recorded curve at 0.01 T. The local maximum shows all characteristics of an antiferromagnetic transition which is in accordance with previous results [3] but there are no clear signs for a second transition which could be expected as both compounds with adjacent stoichiometries ($x=2$ and $x=3$) exhibit a second transition.

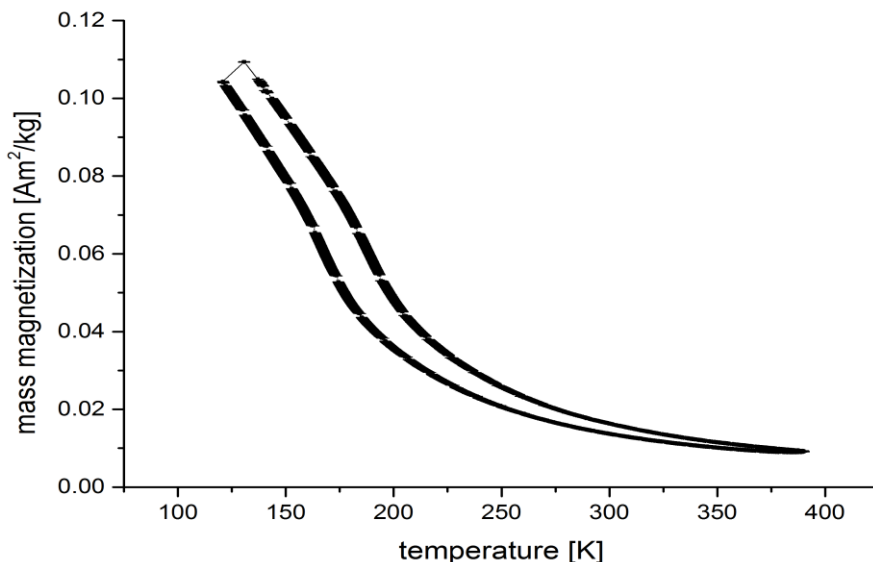


Figure 22. Isofield curve of $\text{Mn}_{2.5}\text{Fe}_{2.5}\text{Si}_3$ at 0.01 T. Data points below 150 K were not measured due to instrumental problems.

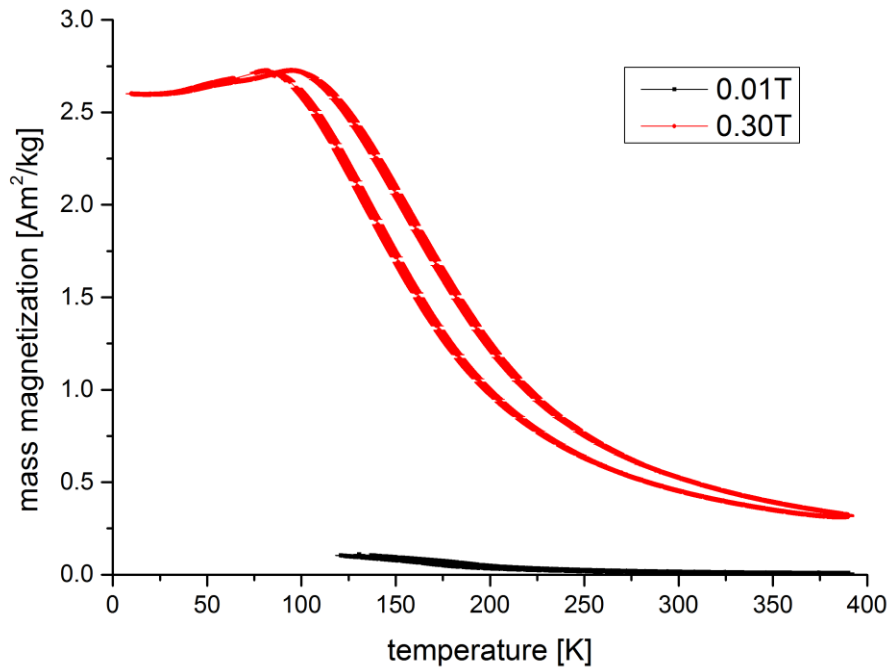


Figure 23. Isofield curves of $\text{Mn}_{2.5}\text{Fe}_{2.5}\text{Si}_3$ at 0.01 T and 0.30 T.

With increasing fields the slight increase towards the maximum more and more gets smeared out and almost vanishes completely (Figure 24). The transition temperature which is characterized by the local maximum does not depend on the external magnetic field and stays constant within the uncertainty of the measurement (Figure 25). The maximum mass magnetization is nearly directly proportional to the field and increases from $2.6 \text{ Am}^2/\text{kg} \pm 0.1 \text{ Am}^2/\text{kg}$ for a field strength of 0.01 T to $14.2 \text{ Am}^2/\text{kg} \pm 0.2 \text{ Am}^2/\text{kg}$ for a field strength of 1.8 T. All curves show a thermal hysteresis starting around a temperature of 15 K then reaching a maximum of $20 \text{ K} \pm 2 \text{ K}$ (0.3 T) around the inflection point of the decreasing part of the curves and then narrowing down again towards higher temperatures. Within the error the maximum splitting of the hysteresis is not field dependent(see Fig. 30 later).

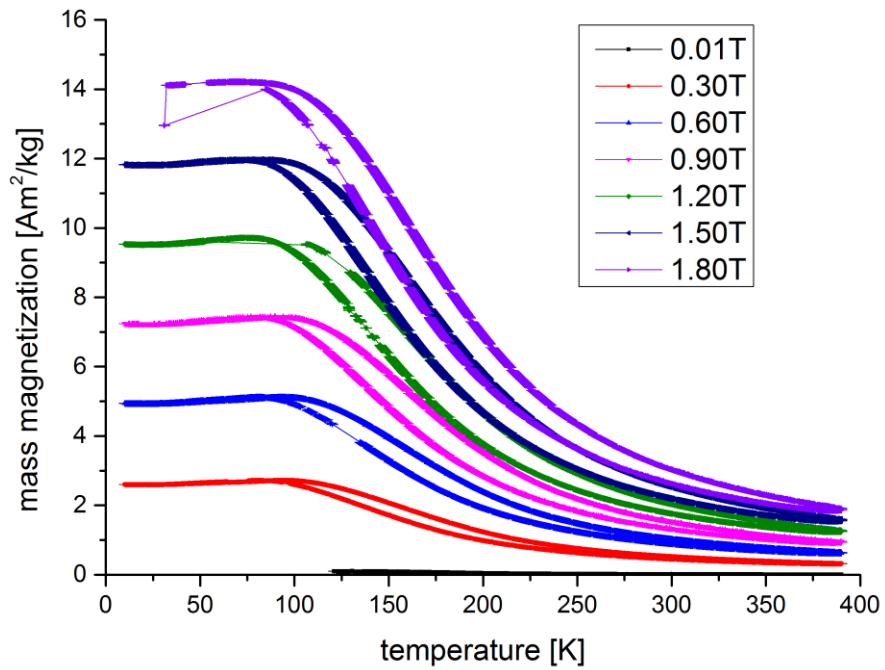


Figure 24. Isofield curves of $\text{Mn}_{2.5}\text{Fe}_{2.5}\text{Si}_3$ in different external magnetic fields.

A plot of the isothermal measurements on the compound $\text{Mn}_{2.5}\text{Fe}_{2.5}\text{Si}_3$ can be seen in Fig.26. All three measured curves are at temperatures above the transition temperature of the material and show paramagnetic behavior. This can be seen in the constant slope of the curves that is higher for curves at lower temperatures. In the measured field range one cannot observe further field driven transitions or hysteretic behavior.

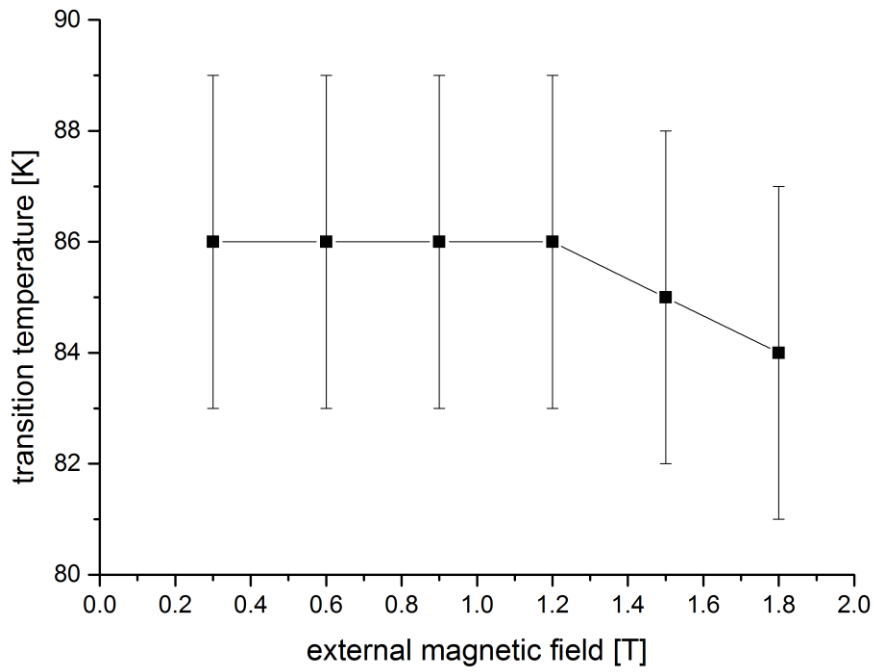


Figure 25. Transition temperatures of the antiferromagnetic transition in $\text{Mn}_{2.5}\text{Fe}_{2.5}\text{Si}_3$ and its dependency on the external magnetic field.

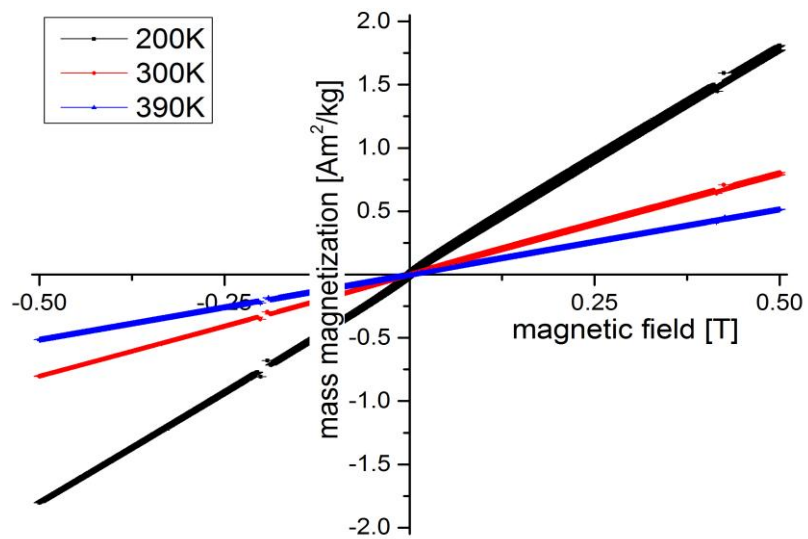


Figure 26. Isothermal curves of $\text{Mn}_{2.5}\text{Fe}_{2.5}\text{Si}_3$ at different temperatures.

4.4 Discussion of magnetic properties of $\text{Mn}_{1.5}\text{Fe}_{3.5}\text{Si}_3$

For the composition $\text{Mn}_{3.5}\text{Fe}_{3.5}\text{Si}_3$ we again start describing the magnetic properties on the basis of the data corresponding the lowest measured external field of 0.01 T. It looks very similar to the curve at 0.3 T from $\text{Mn}_{2.5}\text{Fe}_{2.5}\text{Si}_3$ but shows a flatter increase of the mass magnetization below the local maximum at $214 \text{ K} \pm 3 \text{ K}$. The local maximum also is less sharp and the flattening at high temperatures is more pronounced. The overall shape of the curve shows antiferromagnetic characteristics but less pronounced as for the manganese rich samples. The almost flat behavior below the transition, the flattening at high temperatures and the fairly steep decrease in between could also be indicative of a weak ferromagnet.

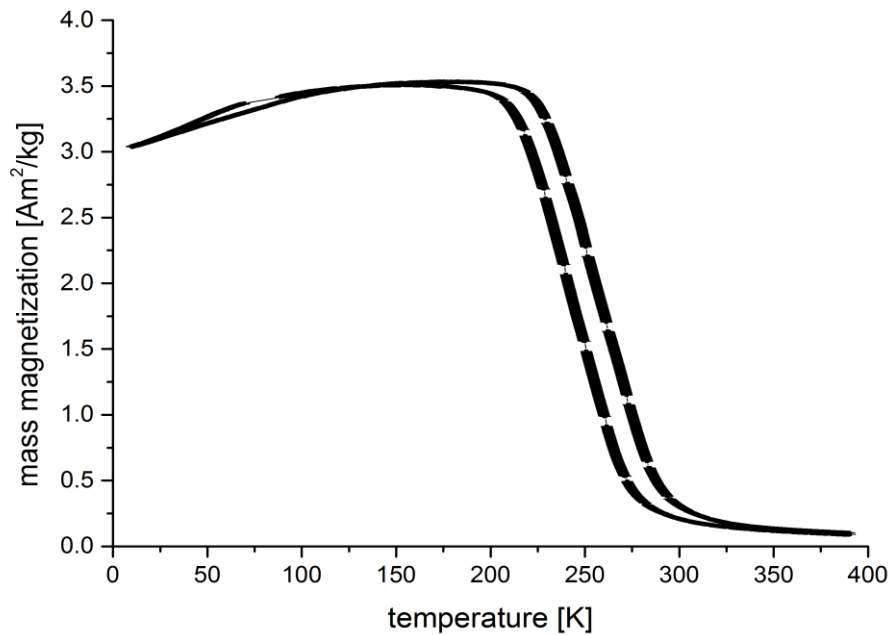


Figure 27. Isofield curve of $\text{Mn}_{1.5}\text{Fe}_{3.5}\text{Si}_3$ at 0.01 T.

With higher fields the ferromagnetic characteristics get more and more pronounced. . A possible explanation is that at low field the compound orders antiferromagnetically and that with the appliance of higher fields the compound turns into a weak ferromagnet. This is also in accordance with the earlier reported

magnetic phase diagram, as the stoichiometry of this sample lies between the one of a antiferromagnet ($\text{Mn}_2\text{Fe}_3\text{Si}_3$) and a ferromagnet (MnFe_4Si_3). With increasing fields the local maximum strongly shifts towards lower temperatures while the flattening happens at higher temperatures. Thus, with higher fields the decreasing part in the intermediate temperature range is much broader. Assuming ferromagnetic characteristics above 0.3 T the inflection point characterizing the ferromagnetic transition temperature increases with rising field strength. For this sample there is no linear dependency of maximum mass magnetization and applied magnetic field. Instead the mass magnetization strongly increases from 0.01 T to 0.3 T, while at higher fields the relative increase gets smaller.

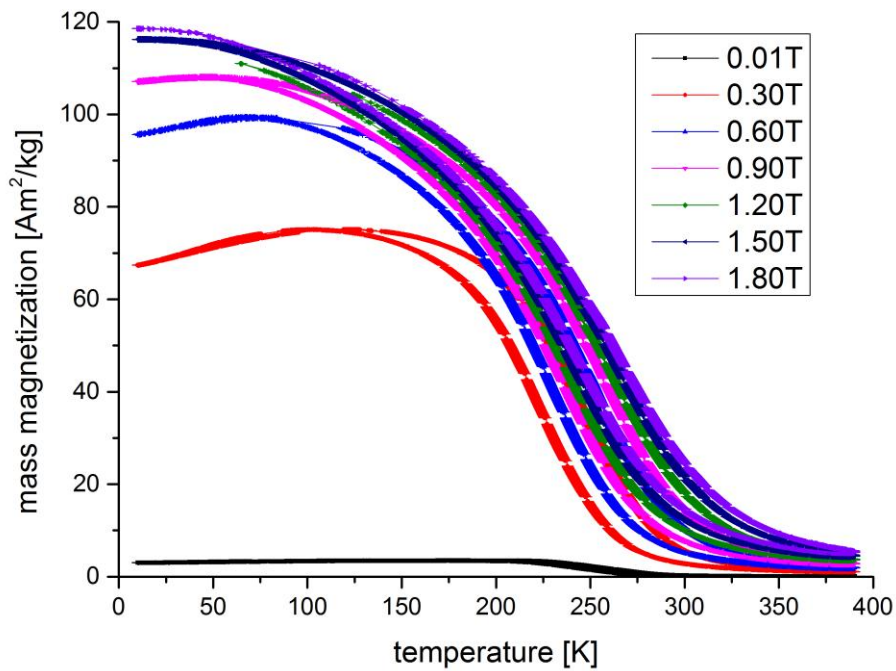


Figure 28. Isofield curves of $\text{Mn}_{1.5}\text{Fe}_{3.5}\text{Si}_3$ in different external magnetic fields.

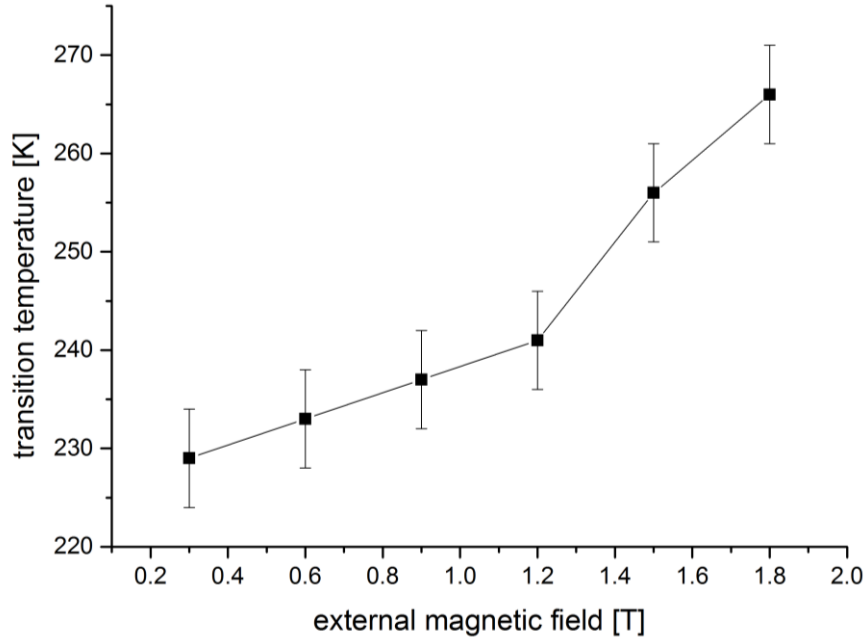


Figure 29. Inflection Points of the isofield curves of $\text{Mn}_{1.5}\text{Fe}_{3.5}\text{Si}_3$ possible corresponding to a ferromagnetic transition temperature.

All isofield curves show strong hysteretic behavior. The maximum hysteresis undergoes a jump from 0.01 T to 0.3 T and remains basically constant for higher fields. This can be seen in Fig. 30.

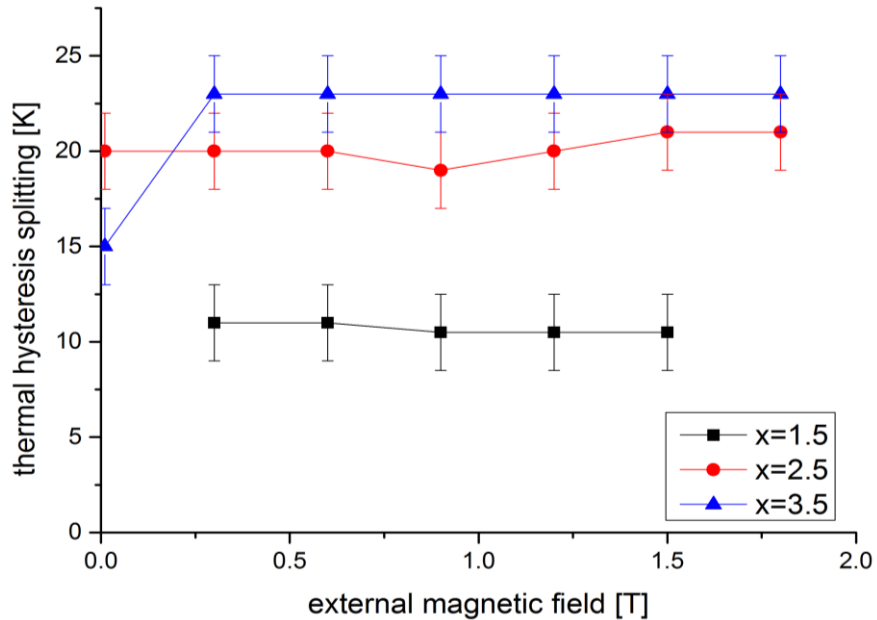


Figure 30. Field dependency of the maximum thermal hysteresis splitting of all measured samples.

The measured isothermal curves for $\text{Mn}_{3.5}\text{Fe}_{3.5}\text{Si}_3$ show two distinct characteristics as in this case the transition temperature of the sample lies in the covered temperature range. The two curves at high temperatures 300 K and 390 K are above the magnetic transition and show paramagnetic behavior. The curve at 200 K is below the magnetic ordering temperature and shows ferromagnetic characteristics, like a beginning saturation for field strengths above 0.25 T and a tiny but observable hysteresis.

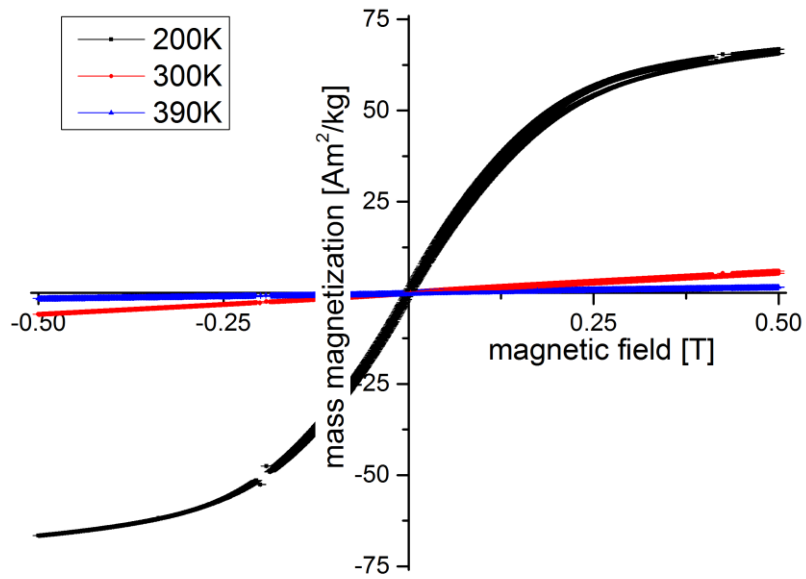


Figure 31. Isothermal curves of $\text{Mn}_{1.5}\text{Fe}_{3.5}\text{Si}_3$ at different temperatures.

5. Conclusions

We want to conclude by setting this work into the context of previously published results.

Our summarized results based on the magnetic measurements on compounds in the series $Mn_{5-x}Fe_xSi_3$ with $x=1.5, 2.5$ and 3.5 are shown in tab. 3.

Mag.T	X=1.5			X=2.5		X=3.5	
	hyst. split.	T ₁	T ₂	hyst. split.	T	hyst. split.	T
0.01T	0.0K±1K	85±3K	119±3K	20K±2K	N/A	15K±2K	214±5K
0.3T	11.0K±2K	81±3K	115±5K	20K±2K	86±3K	23K±2K	229±5K
0.6T	11.0K±2K	84±3K	111±5K	20K±2K	86±3K	23K±2K	233±5K
0.9T	10.5K±2K	88±3K	119±5K	19K±2K	86±3K	23K±2K	237±5K
1.2T	10.5K±2K	88±3K	111±5K	20K±2K	86±3K	23K±2K	241±5K
1.5T	10.5K±2K	85±3K	110±5K	21K±2K	85±3K	23K±2K	256±5K
1.8T	N/A	N/A	N/A	21K±2K	84±3K	23K±2K	266±5K

Table 3. Table of all summarized transition temperatures and thermal hysteresis splittings for the compounds $Mn_{3.5}Fe_{1.5}Si_3$, $Mn_{2.5}Fe_{2.5}Si_3$ and $Mn_{1.5}Fe_{3.5}Si_3$.

We combined our results with the transition temperatures provided in the earlier publication (table 4) which contains data for the compounds with integer values for x [3]. This way we obtained an advanced phase diagram for the whole series.

X	transition temperature T ₁	transition temperature T ₂
X=0	64K	100K
X=1	64.5K	94K
X=2	65 K	127 K
X=3	40 K	250 K
X=4	300 K	
X=5	370 K	

Table 4. Table of transition temperatures from [3].

This advanced phase diagram which now contains data for 9 different stoichiometries is shown in fig. 32. It can be seen that our results fit very nicely in the context of the previous results. Still, there are some interesting details which deserve special mention. First of all, we found magnetic phase transitions in all measured samples. The two antiferromagnetic transitions of $\text{Mn}_{3.5}\text{Fe}_{1.5}\text{Si}_3$ perfectly fill the gap in between the adjacent compounds Mn_4FeSi_3 and $\text{Mn}_3\text{Fe}_2\text{Si}_3$.

$\text{Mn}_{2.5}\text{Fe}_{2.5}\text{Si}_3$, however, undergoes only one phase transition while both adjacent compounds with $x=2$ and $x=3$ undergo two phase transitions. The transition temperature we found fits more to the lower transition temperatures of the other two compounds, but it is slightly increased. $\text{Mn}_{1.5}\text{Fe}_{3.5}\text{Si}_3$ lies in between a antiferromagnetic and a ferromagnetic compound and therefor shows characteristics of both magnetic orderings. If we assume a ferromagnetic transition the transition temperature is slightly lower than the one of $\text{Mn}_2\text{Fe}_3\text{Si}_3$ but not too far off the connection between $x=3$ and $x=4$. If we would assume an antiferromagnetic transition the transition temperature would not fit to the previous results – a fact which further supports the hypothesis of ferromagnetic ordering for the compound.

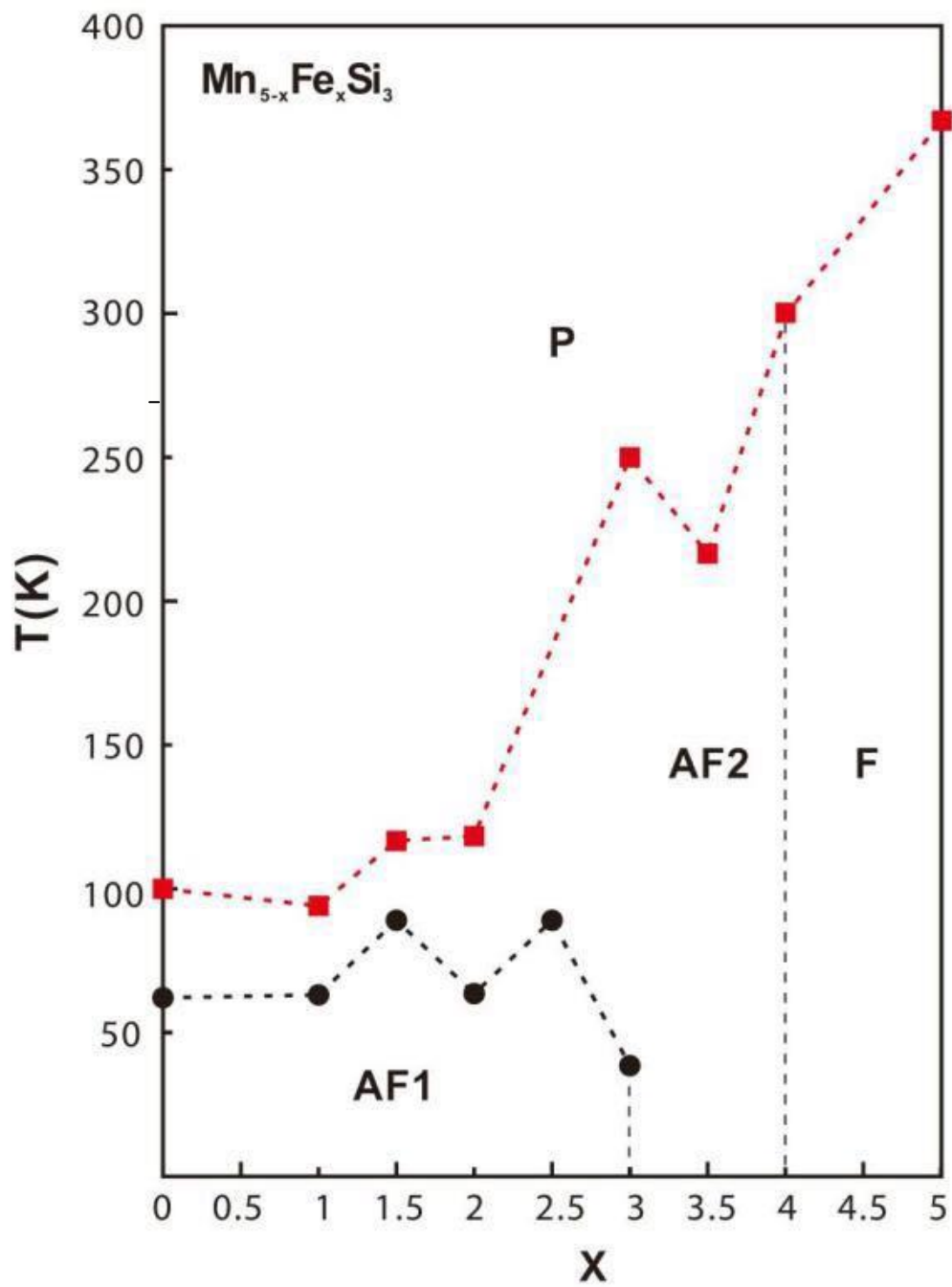


Figure 32. Transition temperatures of the $\text{Mn}_{5-x}\text{Fe}_x\text{Si}_3$ series for compounds $x=0, 1, 1.5, 2, 2.5, 3, 3.5, 4$ and 5 . [3]

Acknowledgements

This work was completed since July, 2015 to August, 2016 in Jülich Research Center, Germany. With this chance, I want to express my thanks to all the following persons, who really provided me great support during this year.

Prof. Dr. Arnold Förster

As the primary mentor of my Bachelor thesis, I appreciate him for suggesting me many useful opinions from a professional and a physics related angle. His ideas showed me a clear direction during this thesis.

Dr. Habil. Karen Friese

Her nice personality made me feel warm like in a big family. Her supervision of this work helped me a lot to finish it. Most importantly I would like to thank you for the interview and provide the position to enable my thesis here in JCNS-2.

Paul Hering

As the person who stayed with me closest from the very first day to the very last day of this work, I am so thankful to him for his patience and powerful background knowledge as well as his experimental ability. I got so much direct and honest support from him all the way. Thank you once more, Paul.

Dr. Jörg Voigt

To the chapter “Results and the Analysis”, Jörg gave me many good advice. During the time when Paul was not there he helped me to carry out measurements.

Prof. Thomas Brückel

As well I want to appreciate Prof. Brückel, realize the possibility for my work in Centre for Neutron Science of Jülich Research Centre, Peter Grünberg Institut, a department to Nobel physic price in 2005.

There are also some nice guys besides the persons above, who I even don't know their names, but also supported me for this work. Just as I imaged before, it really makes fun to complete my Bachelor thesis here in Peter Grünberg Insitut, and it is also an great honor for all my life.

Bibliography

- [1] Gschneidner, K. A., Jr; Pecharsky, V. K. Thirty years of near room temperature magnetic cooling: Where we are today and future prospects. *Int. J. Refrig.* 2008, 31, 945-961.
- [2] Tishin, A. M.; Spichkin, Y. I. The Magnetocaloric Effect and its Applications. *Institute of Physics Series in Condensed Matter Physics.*
- [3] Songlin; Dagula; Tegus, O.; Brueck, E.; Klaasse, J. C. P.; de Boer, F. R.; Buschow, K. H. J. Magnetic phase transition and magnetocaloric effect in $Mn_{5-x}Fe_xSi_3$. *J. Alloys Compd.* 2002, 334, 249–252.
- [4] Wu, X., Zhao, B. Development of Room-Temperature Magnetic Refrigerants. *J. of Magn. Mat. And Devices.* 2003, Vol 34 No.03
- [5] Min, L.; Bingfeng, Y.; Zhangbao, H. Research on performance of regenerative room temperature magnetic refrigeration cycle. *Magn. Refrigeration J.* 2006, 29(8), 1348-1357.
- [6] Yuriy Mozharivskiy, Analogy between magnetic refrigeration and vapor cycle
<http://www.chemistry.mcmaster.ca>
- [7] <http://www.madsci.org>
- [8] Jr; Pecharsky, V. K.; Gschneidner, K. A. Giant Magnetocaloric Effect in $Gd_5(Si_2Ge_2)$. *Phys. Rev. Let.* 1997, 78(23), 4494-4497.
- [9] Binczycka, H.; Dimirijevic, Z.; Gajic, B.; Szytula, A. Atomic and Magnetic Structure of $Mn_{5-x}Fe_xSi_3$. *Phys. stat. sol.* 1973, 19, K13-K17.
- [10] Hering, P.; Friese, K.; Voigt, J.; Persson, J.; Aliouane, N.; Grzechnik, A.; Senyshyn, A.; Brückel, T. Structure, Magnetism, and the Magnetocaloric Effect of $MnFe_4Si_3$ Single Crystals and Powder Samples. *Chem. Materials.* 2015, 27(20), 7128-7136.
- [11] Lincoln Lab's Foner, 82, and Sandholm, 76, MIT News,
<http://news.mit.edu>

- [12] PPMS Vibrating Sample Magnetometer Application Note, Rev 05.09
- [13] Quantum Design. *Vibrating Sample Magnetometer (VSM) Option User's Manual.*, 1096-100, Rev. B0 1-3 February 2011.
- [14] Gier, H. *Kalt-Schmelz-Tiegel*. Eur. Pat. EP 0 345542 B1, 1993.
- [15] Quantum Design. *MulitVu Software*. Release 1.2.3.28
- [16] OriginLab. *OriginPro Software, Version 9.0*. 2012.

